J Mater Sci: Mater Med (2007) 18:661–668
DOI 10.1007/s10856-007-2317-1

Mechanical properties and apatite forming ability of TiO_2 nanoparticles/high density polyethylene composite: Effect of filler content

Masami Hashimoto · Hiroaki Takadama · Mineo Mizuno · Tadashi Kokubo

Received: 23 December 2004 / Accepted: 21 October 2005

Abstract Composite materials consisting of TiO_2 nanoparticles and high-density polyethylene (HDPE), designated hereafter as TiO_2/HDPE, were prepared by a kneading and forming process. The effect of TiO_2 content on the mechanical properties and apatite forming ability of these materials was studied. Increased TiO_2 content resulted in an increase in bending strength, yield strength, Young's modulus and compressive strength (bending strength = 68 MPa, yield strength = 54 MPa, Young's modulus = 7 GPa, and compressive strength = 82 MPa) at 50 vol% TiO_2. The composite with 50 vol% TiO_2 shows a similar strength and Young's modulus to human cortical bone. The TiO_2/HDPE composites with different TiO_2 contents were soaked at 36.5 °C for up to 14 days in a simulated body fluid (SBF) whose ion concentrations were nearly equal to those of human blood plasma. The apatite forming ability, which is indicative of bioactivity, increased with TiO_2 content. Little apatite formation was observed for the TiO_2/HDPE composite with 20 vol% content. However, in the case of 40 vol% TiO_2 content and higher, the apatite layers were formed on the surface of the composites within 7 days. The most potent TiO_2 content for a bone-repairing material was 50 vol%, judging from the mechanical and biological results. This kind of bioactive material with similar mechanical properties to human cortical bone is expected to be useful as a load bearing bone substitute in areas such as the vertebra and cranium.

M. Hashimoto · H. Takadama (✉) · M. Mizuno
Japan Fine Ceramics Center, 2-4-1 Mutsuno, Atsuta-ku, Nagoya 456-8587, Japan
e-mail: masami@jfcc.or.jp

T. Kokubo
Research Institute for Science and Technology, Chubu University, 1200 Matsumoto-cho, Kasugai 487-8501, Japan

Introduction

It has been reported that some ceramics, such as Na_2O-CaO-SiO_2-P_2O_5 glasses [1], sintered hydroxyapatite [2], and glass-ceramics containing crystalline apatite and wollastonite (A–W) [3], can bond to living bone. These ceramics are already clinically used as important bone-repairing materials. Recently, it was also reported that even metals such as titanium and its alloys can bond to living bone when they have been previously subjected to alkali and heat treatment [4] or alkali, water and heat treatment [5]. However, they have much higher elastic moduli than does natural bone. This is a critical problem, since a high elastic modulus of the materials may induce bone resorption because of their stress shielding. On the other hand, polymeric materials generally possess low elastic moduli, but none bond to living bone except for Polyactive™, which is biodegradable [6]. Therefore, new types of materials having a high bioactivity as well as mechanical strengths analogous to those of the natural bone must still be developed for load-bearing bone substitutes.

A composite (HAPEX™) of hydroxyapatite particles with high-density polyethylene (HDPE) was developed in the early 1980s as a bone substitute with analogous mechanical properties to those of the bone [7]. It is already clinically used for artificial incus bones. Some of the mechanical properties of HAPEX™, such as the tensile strength, have already been found to be desirable for its use in the body [8–10]. However, the fracture toughness and elastic modulus of HAPEX™ are lower than those of living bone. Additionally, glass – ceramic A-W-reinforced HDPE was developed in 1998 [11, 12]. The bioactivity of this composite is higher than that of HAPEX™, but its mechanical strengths are lower than that of HAPEX™.

On the other hand, hydroxyapatite-reinforced poly–(L-lactide) (PLLA) [13] has an initial bending strength of

280 MPa, which exceeds the bending strength of the human cortical bone (50 to 150 MPa), and an elastic modulus of 12 GPa, which is in the range of the elastic modulus of the human cortical bone (7 to 30 GPa) [14]. These mechanical properties of this composite, however, decrease to 200 MPa after 25 weeks in the phosphate-buffered saline because of the biodegradability of PLLA. Therefore, this composite is not useful as a load-bearing bone substitute but only for fracture-fixation devices such as pins or screws. Therefore, in order to develop a bone-repairing material with bone-like mechanical properties, it is necessary to incorporate a bioactive ceramic particulate with a high mechanical strength and elastic modulus into a nondegradable ductile matrix.

Kokubo et al. reported that titania gels with an amorphous structure did not induce apatite formation on their surfaces in a simulated body fluid (SBF), which was prepared to have an ion concentration nearly equal to that of human blood plasma (Na^+ 142.0, K^+ 5.0, Ca^{2+} 2.5, Mg^{2+} 1.5, Cl^- 147.8, HCO_3^- 4.2, HPO_4^{2-} 1.0, and SO_4^{2-} 0.5mM) [15], whereas the gels with an anatase or rutile structure induced apatite formation on their surfaces [16–18]. The deposition of apatite was more pronounced on the anatase gels than on the rutile gels. Therefore, a titania with a specific crystal structure, such as anatase, is effective in inducing apatite nucleation in a body environment.

Fillers have an important role in modifying the properties of various polymers. In polymeric materials, inorganic particles are used as fillers to improve their strength, toughness and wear properties [19]. The effect of fillers on the properties of the composites depends on their concentration and particle size and shape, as well as their interaction with the matrix. As yet, there has been no study regarding the effect of TiO_2 on the mechanical strengths of HDPE. TiO_2 has high mechanical strengths. For example, the elastic modulus of TiO_2 (300–320 GPa) is much higher than that of hydroxyapatite (86–110 GPa) [14]. So incorporating TiO_2 particles into the polymer matrix is considered to be effective to enhance the mechanical properties of the polymer matrix.

In this study, the effects of TiO_2 content on the bending, yield strengths, Young's modulus, the strain to failure, and compressive strength of TiO_2/HDPE composite were investigated. In addition, the apatite forming ability of TiO_2/HDPE composite in SBF was studied.

Materials and methods

Materials

Solvents and reagents, all of special reagent grade, were used without further purification. An anatase-type TiO_2 nanopowder was manufactured by Ishihara Sangyo Kaisha, Ltd., Mie, Japan. The phase of the TiO_2 powders was analyzed by powder X-ray diffraction. The TiO_2 particles were analyzed in terms of size using a laser scattering particle size distribution analyzer (MasterSizer 2000, MALVERN Co., Japan) and a BET-specific surface area analyzer (NOVA-2000, Yuasaionics Co., Japan). The surface chemical composition of the outermost layer of the as-received TiO_2 was analyzed by an X-ray photoelectron spectrometer (XPS) with an ESCA LAB MKII Model (VG Scientific, East Grin stead, England). An MgKα X-ray was used as the source. The photoelectron take-off angle was set at 30°. The measured binding energy was corrected by referring to that of the C1s as 285.0 eV. The zeta potential of the surface of the as-received TiO_2 was measured by laser electrophoresis with a Penmkem 501 Model in 0.01 mol/l phosphate buffer saline of pH 7.2 at 20 °C.

HDPE (Japan Polyolefins Co., Ltd., Tokyo, Japan) had the following number-average molecular weight: Mn, weight-average molecular weight in 1.2×10^4; Mw in 7.67×10^4 and z-average molecular weight; Mz in 47.6×10^4, Mw/Mn in 6.35 and Mz/Mw in 6.20. The melt flowing rate (MFR) of this polyethylene is 8.

Preparation of TiO_2/HDPE composites

The manufacturing process of the TiO_2/HDPE involved kneading and compression moulding. The filler content was set at 20, 40, 45, 50, 52, 52.5 and 55.6 vol%. These composites were denoted as TiO_2/HDPE −20, 40, 45, 50, 52, 52.5 and 55.6, respectively. HDPE was dried at 80 °C for 8 h and then kneaded at 210 °C in a batch kneader PBV 0.3 (Irie Seisaku-sho, Ltd., Tokyo, Japan). TiO_2 particles were added slowly into the melted HDPE with kneading at 210 °C in air. After adding TiO_2, the TiO_2/HDPE compound was kneaded with a 25 rpm rotation speed for 30 min.

The obtained compounds were molded at 230 °C for 1 h and then hot-pressed in air under a pressure of 2.5 MPa.

Characterization of TiO_2/HDPE composites

Mechanical test

Three-point bend testing of TiO_2/HDPE composites was performed using ten samples of each type of composite. The specimens were cut to the desired shape and then polished, using 400 grit silicon carbide paper, to a size of 40 mm × 10 mm × 4 mm. A testing machine, Model 5582 (Instron Co. Ltd., L. A., USA), was used to apply a load over a 30 mm span. Measurements were performed with a cross-head speed of 1.0 mm/min at room temperature according to JIS K 7171. The fracture surfaces were examined using a field emission scanning electron microscope (FE-SEM)

with a JSM-633OF Model (JEOL DATUM Co. Ltd., Nagoya, Japan) after coating with a thin layer of Au.

The values for bending strength, Young's modulus, yield strength and strain to failure were calculated according to the following equations: [12, 20]

$$\text{Bending strength } \sigma = 3pL/2bd^2 \quad (1)$$

$$\text{Young's modulus } E = \sigma/(6d\delta/L^2) \quad (2)$$

$$\text{Yield strength } \sigma_f = (3p_fL/2bd^2)((n+2)/3) \quad (3)$$

$$\text{Strain to failure } \varepsilon = (6d\delta/L^2)((2n+1)/n)(1/3), \quad (4)$$

where p is the load at elastic limit (N), p_f is the load at fracture (N), L is the sample length (mm), δ is the displacement of the cross head (mm), b is the sample width (mm), d is the sample height (mm) and n is a strain-hardening exponent ($0 < n < 1$).

For compressive mechanical analysis, specimens of the dimensions 10 mm × 10 mm × 4 mm were cut from the hot-pressed composite plates. They were subsequently polished using 400 grit silicon carbide papers to remove defects from the specimen surfaces. The strength measurement was carried out at a cross-head speed of 1.0 mm/min according to JIS K 7181. The tests were carried out at room temperature in air.

The compressive strength was calculated from

$$\text{Compressive strength, } \sigma_f = F/A, \quad (5)$$

where F is fracture load (N) and A is the initial cross sectional area (mm^2).

Density

The densities of the TiO_2/HDPE composites were measured by the Archimedes method using a pycnometer and a glass bottle of known volume with a capillary tube at the top as a container. The liquid medium for all materials was distilled water.

Bioactivity test

The bioactivity of the TiO_2/HDPE composites was evaluated by examining apatite formation on their surfaces in the simulated body fluid (SBF). It has been revealed that materials that form a bone-like apatite on their surfaces in SBF form the apatite even in a living body and bond to living bone through the apatite layer [21]. The bioactivity of the composite was compared with that of TiO_2 particles or pure HDPE. The TiO_2 particles were embedded on the tape stuck to a glass slide 10 mm × 10 mm × 2 mm in size. For both HDPE and TiO_2/HDPE composites, specimens of 10 mm × 10 mm × 4 mm in size were cut, polished with a 400 grit silicon carbide paper for 5 min, washed with distilled water and dried at room temperature. SBF with ion concentrations nearly equal to those of human blood plasma was prepared by dissolving the reagents NaCl, $NaHCO_3$, KCl, $K_2HPO_4{\cdot}3H_2O$, $MgCl_2{\cdot}6H_2O$, $CaCl_2$ and Na_2SO_4 (Nacalai tesque, Inc. Kyoto, Japan) in distilled water and buffered at pH7.4 and 36.5 °C with $(CH_2OH)_3CNH_2$ and 1M HCl (Nacalai tesque, Inc. Kyoto, Japan). The specimens were soaked in 30 ml of SBF at 36.5 °C. After various time periods, the specimens were removed from the fluid, washed moderately with ion-exchanged distilled water, and dried at room temperature for 1 day. Their surfaces were analyzed by thin-film X-ray diffraction (TF-XRD) with RINT Model 2000 (Rigaku Denki Co. Ltd., Tokyo, Japan). The morphology of the surface layer of the composites was observed by FE-SEM after coating them with a thin Au film.

Results

Characterization of TiO_2

The as-received TiO_2 particles were confirmed to be essentially of the anatase phase by powder X-ray diffraction analysis. They had a broad particle size distribution, with a median particle size of 535 nm. The BET surface area of the as-received TiO_2 was approximately 8.56 m^2g^{-1}. Figure 1 shows a TEM photograph of the as-received TiO_2. TiO_2 particles possessed a round shape and smooth surface. Figure 2 shows O(1s) spectra of the as-received TiO_2. Both TiO_2 and Ti-OH peaks were detected. This result indicates that the as-received TiO_2 already has Ti-OH groups, which is essential for apatite nucleation. The zeta potential of the surface of the as-received TiO_2 was found to be highly negative (−22.5 mV).

Fracture surface of composites

Figure 3 shows FE-SEM images of the fracture surfaces of TiO_2/HDPE composites with different TiO_2 contents after the bending test. As the FE-SEM image in Fig. 3a shows, at 20 vol% filler content there was a large degree of polymer deformation; this was indicated by the presence of elongated strands of polyethylene. However, with greater than 40 vol% of TiO_2 (Figs. 3b,c and d), there was a small degree of polymer deformation. Along with the formation of polymer fibrils, the particles of TiO_2 were still clearly seen within the polyethylene matrix. It was easy to detect the TiO_2 agglomerates in the TiO_2/HDPE-52 (Fig. 3c) and TiO_2/HDPE-56 (Fig. 3d).

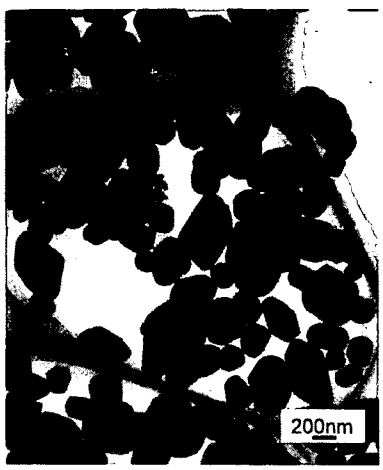

Fig. 1 Transmission electron micrograph of the as-received TiO_2 particles

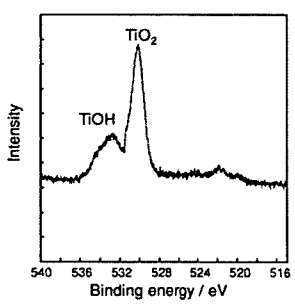

Fig. 2 O(1s) peak in the XPS spectrum of as-received TiO_2

Mechanical properties of composites

The values for bending strength, yield strength, Young's modulus, fracture strain and compressive strength of the TiO_2/HDPE composites and HDPE are shown in Table 1. The bending strength, yield strength and Young's modulus increased with increasing TiO_2 content up to 50 vol% and decreased with increasing content above 52 vol%. The yield strength and Young's modulus were, respectively, 28 MPa and 1.4 GPa for HDPE, 49 MPa and 7.6 GPa for TiO_2/HDPE-40, 54 MPa and 7.1GPa for TiO_2/HDPE-50, and 29 MPa and 6.8 GPa for TiO_2/HDPE-55.6. The strain to failure decreased as the TiO_2 content increased up to 40 vol%. However, the values obtained for the strain to failure increased for the composites with a TiO_2 content higher than 45 vol%.

The increase in the TiO_2 volume fraction resulted in an increase in compressive strength. The following compressive strengths were obtained: 22 MPa for HDPE, 61 MPa for TiO_2/HDPE-40, 75 MPa for TiO_2/HDPE-50, and 87 MPa for TiO_2/HDPE-55.6.

The representative load-displacement curves of three-point bend testing were demonstrated for TiO_2/HDPE composites in Fig. 4. Figure 4 shows that HDPE did not fracture within the limits of the three-point bending apparatus. This behavior resulted in mechanical properties, in that they had a low bending strength, yield strength and Young's modulus, and a large strain to failure. For TiO_2/HDPE-20 and TiO_2/HDPE-40, this ductile behavior was no longer a dominant feature. As the TiO_2 content increased from 40 vol%, the fracture strain also increased.

Density of composites

Figure 5 shows the densities of TiO_2/HDPE composites. Compared to the theoretical density, which was calculated by the rule of mixture, the density of TiO_2/HDPE composites with a low TiO_2 content (20 vol%) almost matched the theoretical value. However, as the amount of TiO_2 was increased up to 55.6 vol%, the discrepancy between the measured and theoretical densities increased.

Bioactivity of composites

Figure 6 shows TF-XRD patterns of TiO_2 particle (a) and HDPE (b) which were soaked in SBF for 3 and 14 days, respectively. Apatite was able to form on the TiO_2 particles after 3 days of soaking; however, it was not formed on the HDPE even after 14 days of soaking in SBF.

Figure 7 shows TF-XRD patterns of TiO_2/HDPE composites that were soaked in SBF for 14 days. Apatite peaks were detected on all of the TiO_2/HDPE composites except for those with 0 and 20 vol% of TiO_2. This result indicates that the apatite forms on TiO_2/HDPE composites with a TiO_2content greater than 40 vol% in SBF and that apatite-forming ability increases with increasing TiO_2 content. Figure 8 shows TF-XRD patterns of a TiO_2/HDPE composite with 50 vol% of TiO_2 that was soaked in SBF for various periods up to 14 days. Small apatite peaks were detected at 7 days of soaking. With 14 days of soaking, these apatite peaks increased. This result indicates that the apatite formed on a TiO_2/HDPE composite with 50 vol% of TiO_2 increased with increasing soaking time.

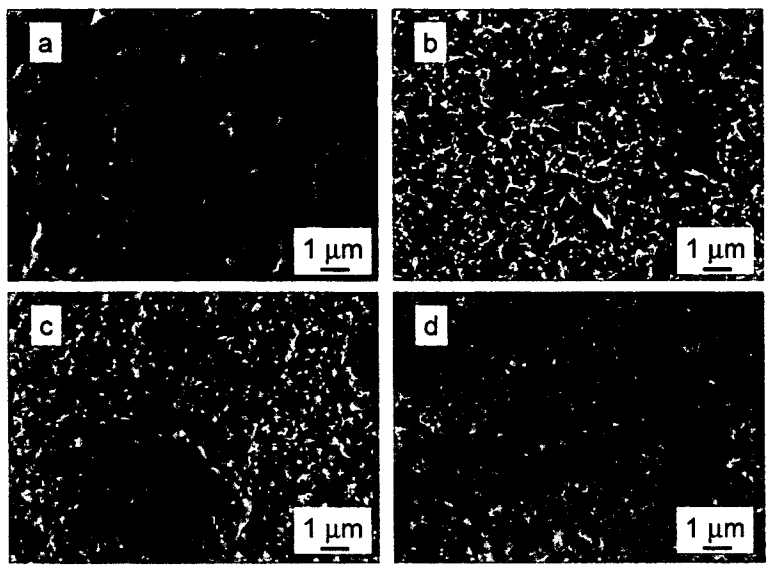

Fig. 3 Scanning electron micrographs of fracture surfaces of TiO_2/HDPE composites —20 (a), 40 (b), 52 (c) and 55.6 vol% (d)

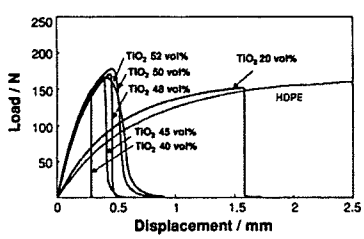

Fig. 4 Load-displacement curves for TiO_2/HDPE composites

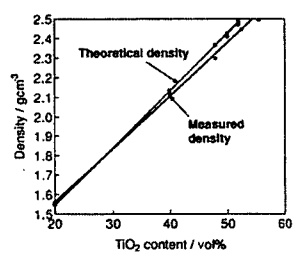

Fig. 5 Density of TiO_2/HDPE composites as a function of the TiO_2 content

Figure 9 shows FE-SEM photographs of the TiO_2/HDPE composite with 50 vol% of TiO_2 that was soaked in SBF at 36.5 °C for various periods shorter than 14 days. No crystals were formed on the TiO_2/HDPE (Fig. 9b) surfaces after soaking in SBF for 5 days. The TiO_2/HDPE surface was covered with hemispherical particles around several micrometers in diameter after 7 days of soaking in SBF (Fig. 9c), and the number and size of the apatite nuclei increased with increasing soaking time (Fig. 9d). The morphology of the apatite on the TiO_2/HDPE composite was polycrystalline fine particles.

Discussion

The results shown here demonstrate that only the 20 vol% TiO_2 incorporation into the HDPE matrix was effective in enhancing the mechanical strengths of the HDPE. The reason for this effect is that the high mechanical strength of TiO_2 (Young's modulus 300–320 GPa) and its smaller particle size allow for a greater surface area to be available

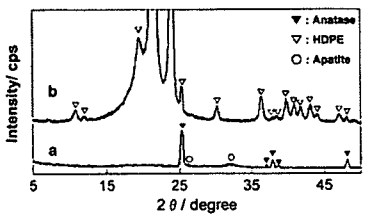

Fig. 6 TF-XRD patterns of the surfaces of TiO_2 particles (a) and HDPE (b) soaked in SBF at 36.5 °C for 3 and 14 days, respectively

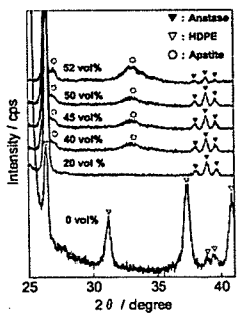

Fig. 7 TF-XRD patterns of the surfaces of TiO_2/HDPE –x composites soaked in SBF at 36.5 °C for 14 days (X = 0, 20, 40, 45, 50, 52 vol%)

for polymer/filler interaction and adhesion. The bending strength, yield strength and Young's modulus increased with increasing filler content, but they decreased when the filler content was greater than 52 vol%. Achieving a homogeneous dispersion of nanoparticles in a polymeric matrix is very difficult due to the strong tendency of nanoparticles to agglomerate [22]. Consequently, nanoparticle-filled polymers are liable to form a number of loosened clusters of particles. Figures 3c and d show TiO_2 aggregate in the HDPE matrix. These agglomerated for the composites with a TiO_2 content greater than 52 vol% and decreased the bending strength, yield strength and Young's modulus.

TiO_2/HDPE-20 and −40 also exhibited a much smaller plastic region after yielding, indicating that the interfacial bond between TiO_2 and HDPE was weak. As mentioned previously, TiO_2 nanoparticles (Fig. 1) had loosened clusters created by the aggregation of smaller TiO_2 particles this is shown in Figs. 3c and d. This structure caused a higher strain to failure due to an increase in crack deflection with increasing particle size of the composite with larger than 40 vol% TiO_2. For TiO_2/HDPE composites, no residual polyethylene

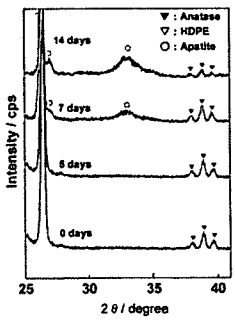

Fig. 8 TF-XRD patterns of the surfaces of TiO_2/HDPE-50 soaked in SBF at 36.5 °C for various periods

was found on the TiO_2 particle surfaces, indicating that no chemical bond existed between the matrix and filler (Fig. 3). Therefore, the voids form at the particle matrix interface, first in the direction of the applied stress (Fig. 5). This void then grows and merges as shear stresses deform the rest of the matrix, leading to the eventual failure of the composites. This result is consistent with the model proposed by Juhasz et al. for an apatite-wollastonite reinforced HDPE composite with no interfacial bonding [12].

Bonfield et al. developed hydroxyapatite-reinforced HDPE composite (HAPEX™) as an analogue material for bone replacement [7–10].The closer Young's modulus matching of the material to bone is an important factor in solving the problem of bone resorption. The fracture toughness and Young's modulus of HAPEX™ have a lower value than those of the human cortical bone.

The yield strength (50 MPa) and Young's modulus (7 GPa) for TiO_2/HDPE-40 were much larger than those for the HAPEX™ with 40 vol % of hydroxyapatite (28 MPa and 4.1 GPa, respectively). It has been generally observed that the addition of ceramic filler can substantially improve the mechanical strengths of the polyethylene. The mechanism of the reinforcing action is as follows. Inorganic fillers are actually bonded to the macromolecular chains and thereby immobilize the polymer chains. The degree of adhesion between the polymer matrix and fillers, the surface area of the filler, and the packing characteristics of the filler particles are important factors that determine the mechanical properties of the composites [23–25]. Comparing TiO_2 with hydroxyapatite as a ceramic filler, the surface area (8.56 m^2g^{-1}) and average particle size (535 nm) of TiO_2 were much larger and lower than those of hydroxyapatite [7] (7.61 m^2g^{-1} and 7.3 μm, respectively). TiO_2(40 vol%) homogeneously dispersed in the HDPE matrix via the kneading and compacting of TiO_2

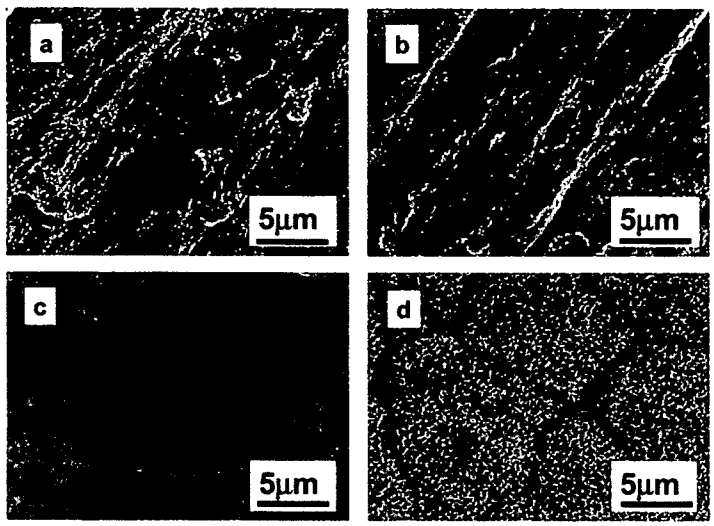

Fig. 9 Scanning electron micrographs of the surfaces of the TiO_2/HDPE-50 composite soaked in SBF at 36.5 °C for various periods: 0 days (a), 5 days (b), 7 days (c) and 14 days (d)

nanoparticles and HDPE (Fig. 3b). Many kinds of polyethylene exist, including ultrahigh molecular weight polyethylene (UHMWPE), HDPE and low density polyethylene (LDPE). Our previous study indicated that the degree of TiO_2 nanoparticle dispersion in the various polyethylene matrixes varied [26–28]. Therefore, the degree of homogeneous dispersion decreased in the order: HDPE (MFR8) > HDPE (MFR20) $\gg$ HDPE (MFR0.3) $\simeq$ HDPE (MFR40) $\gg$ UHMWPE $\simeq$ 0. These results indicate that the HDPE (MFR8) matrixes, in which TiO_2 nanoparticles with a high surface area are homogeneously dispersed have high mechanical properties, and that those with micrometer-sized hydroxyapatite particles eventually have low ones.

Biomineralization processes such as apatite formation are complex and involve the controlled nucleation and growth of apatite from aqueous solutions. Organisms create the proper organic matrix as a host for nucleation and growth, for control of solution concentrations, and for the supersaturation of precipitating phases. Most of the macromolecules known to promote surface nucleation contain functional groups that are negatively charged at pH's where the crystallization occurs [29].

In general, the crystallization of many sparingly soluble salts involves the formation of metastable precursor phases. In the case of calcium phosphate, various metastable phases have been identified. It is believed that the initial formation of an amorphous calcium phosphate may be followed by its transformation to hydroxyapatite. A recent X-ray diffraction crystallographic study by Kokubo showed that the anatase gel induces apatite formation the most effectively, followed by the rutile gel; the amorphous gel, however, forms no apatite [18]. The Ti-OH groups on the anatase gel combine with Ca^{2+} ions in the SBF to form amorphous calcium titanate. This calcium titanate later combines with phosphate ions in the SBF to form amorphous calcium phosphate with a low Ca/P ratio [30, 31]. The calcium phosphate transforms into the apatite, which exhibits a Ca/P ratio of 1.65. This demonstrates that the surface functional groups, which are capable of binding soluble ionic precursors, may become sites for surface nucleation.

The XRD study showed that the apatite formed on all the TiO_2/HDPE composites except for those with 0 and 20 vol % of TiO_2, as exemplified by the composite with 52 vol% of TiO_2 shown in Fig. 7. The induction period of the apatite nucleation was 7 days, as shown in Fig. 8. The as-received TiO_2 has an anatase structure, a Ti-OH group (Fig. 2) and a negative zeta potential (−22.5 mV). Figure 6 shows the apatite formed on the TiO_2 particles after soaking in SBF for as

little as 3 days; however no apatite formed on the polyethylene after soaking in SBF for 14 days. The TiO_2/HDPE surfaces were ground to a 30 μm finish with #400 silicon carbide abrasive paper. This suggests that the HDPE polymer chains were elongated and partially covered the surfaces of the TiO_2 particles. Therefore, the induction period of the apatite formation would be delayed for a longer time than that for TiO_2 particles. To enhance the apatite forming ability of the TiO_2/HDPE composite, it is necessary to remove by surface treatment the polyethylene that covers the TiO_2 particles.

Conclusions

The bending strength, yield strength, Young's modulus and compressive strength increased with increasing TiO_2 content up to 52 vol% (maximum bending strength = 68 MPa, yield strength = 54 MPa, Young's modulus = 7 GPa and compressive strength = 82 MPa). The strain to failure was reduced with increasing TiO_2 up to 40 vol%. However, as the filler content was increased from 45 to 52 vol%, the strain to failure increased due to the larger particle size resulting from the aggregation of TiO_2 nanoparticles. Three-point bending and compressive testing demonstrated that the composites with a filler content between 40 and 50 vol% showed the most suitable mechanical properties for maxillofacial applications. Apatite formed on TiO_2/HDPE that had greater than 40 vol% of TiO_2 after soaking in SBF for 7 days. These results indicate that the TiO_2/HDPE-50 composite is the most promising material in the present study for use as a load-bearing bone substitute.

Acknowledgements This work is in part supported by the National Research & Development Programs for Medical and Welfare apparatus from the New Energy and Industrial Technology Development Organization (NEDO) entrusted to the Japan Fine Ceramics Center.

References

1. L. L. HENCH, R. J. SPLINTER, W. C. ALLEN and T. K. JR. GREENLEE, *J. Biomed. Mater. Res.* 2 (1971) 117.
2. M. JARCHO, J. L. KAY, R. H. GUMAER and H. P. DROBECK, *J. Bioeng.* 1 (1977) 79.
3. T. KOKUBO, M. SHIGEMATSU, Y. NAGASHIMA, M. TASHIRO, T. NAKAMURA, T. YAMAMURO and S. HIGASHI, *Bull. Inst. Chem. Res. Kyoto Univ.* 60 (1982) 260.
4. S. NISHIGUCHI, H. KATO, H. FUJITA, H. M. KIM, F. MIYAJI, T. KOKUBO and T. NAKAMURA, *J. Biomed. Mater. Res.* 48(5) (1999) 689.
5. S. FUJIBAYASHI, T. NAKAMURA, S. NISHIGUCHI, J. TAMURA, M. UCHIDA, H. M. KIM and T. KOKUBO, *J. Biomed. Mater. Res.* 56(4) (2001) 562.
6. C. A. VAN BLITTERSWIJK, D. BAKKER, H. LEENDERS, J. BRINK, S. C. HESSELING, Y. P. BORELL, A. M. RADDER, R. J. SAKKERS, M. L. GAILLARD, P. H. HEINZE and G. J. BEUMER, ed. by P. Ducheyne, T. Kokubo and C. A. Van Blitterswijk, (Reed Healthcare Communications, The Netherlands, 1992) p. 13.
7. W. BONFIELD, M. D. GRYNPAS, A. E. TULLY, J. BOWMAN and J. ABRAM, *Biomaterials* 2 (1981) 185.
8. M. WANG, R. JOSEPH and W. BONFIELD, *Biomaterials* 19 (1998) 2357.
9. M. WANG and W. BONFIELD, *Biomaterials* 22 (2001) 1311.
10. M. WANG, *Biomaterials* 24 (2003) 2133.
11. J. A. JUHASZ, S. M. BEST, W. BONFIELD, M. KAWASHITA, N. MIYATA, T. KOKUBO and T. NAKAMURA, *J. Mater. Sci: Mater. In Med.* 14 (2003) 489.
12. J. A. JUHASZ, S. M. BEST, R. BROOKS, M. KAWASHITA, N. MIYATA, T. KOKUBO, T. NAKAMURA and W. BONFIELD, *Biomaterials* 25 (2004) 949.
13. T. FURUKAWA, Y. MATSUSUE, T. YASUNAGA, Y. NAKAGAWA, Y. OKADA, Y. SHIKINAMI, M. OKUNO and T. NAKAMURA, *J. Biomed. Mater. Res.* 50 (2000) 410.
14. L. L. HENCH and J. WILSON, in "An introduction to bioceramics" (World Scientific Publishing Co, London, 1992) p. 12.
15. T. KOKUBO, H. KUSHITANI and S. SAKKA, *J. Biomed. Mater. Res.* 24 (1990) 721.
16. M. UCHIDA, H. M. KIM, T. KOKUBO and T. NAKAMURA, *J. Am. Ceram. Soc.* 84 (2001) 2969.
17. M. WEI, M. UCHIDA, H. M. KIM, T. KOKUBO and T. NAKAMURA, *Biomaterials* 23 (2002) 167.
18. M. UCHIDA, H. M. KIM, T. KOKUBO and T. NAKAMURA, *J. Biomed. Mater. Res.* 64A (2003) 164.
19. T. P. SELVIN, J. KURUVILLA and T. SABU, *Materials Letters* 58 (2004) 281.
20. N. E. DOWLING, in "Engineering materials for deformation, fracture and fatigue" (Prentice-Hall Inc, Englewood Cliffs, NJ: 1993), p. 570.
21. T. NAKAMURA, M. NEO and T. KOKUBO, in "Mineralization in Natural and Synthetic Biomaterials" ed. by P. Li, P. Calvert, T. Kokubo, R. Levy and C. Sheid (Materials Research Society, Warrendale, PA, 2000) p.15.
22. M. Z. RONG, M. Q. ZHANG, Y. X. ZHENG, H. M. ZENG, R. WALTER and K. FRIEDRICH, *Polymer* 42 (2001) 167.
23. Y. LIU, J. Y. LEE and L. HONG, *J. Power Sources* 109 (2002) 507.
24. C. J. R. VERBEEK, *Materials Letters* 57 (2003) 1919.
25. Z. WEN, T. ITOH, T. UNO, M. KUBO and O. YAMAMOTO, *Solid State Ionics* 8916 (2003) 1.
26. M. HASHIMOTO, H. TAKADAMA, M. MIZUNO, Y. YASUTOMI and T. KOKUBO, *Key Engineering Materials* 240–242 (2003) 415.
27. H. TAKADAMA, M. HASHIMOTO, Y. TAKIGAWA, M. MIZUNO, Y. YASUTOMI and T. KOKUBO, *Key Engineering Materials* 240–242 (2003) 951.
28. H. TAKADAMA, M. HASHIMOTO, Y. TAKIGAWA, M. MIZUNO, Y. YASUTOMI and T. KOKUBO, *Key Engineering Materials* 254–256 (2004) 569.
29. S. WEINER, *CRC Crit. Rev. Biochem.* 20 (1986) 365–408.
30. H. TAKADAMA, H. M. KIM, T. KOKUBO and T. NAKAMURA, *J. Biomed. Mater. Res.* 55 (2001) 185.
31. H. TAKADAMA, H. M. KIM, T. KOKUBO and T. NAKAMURA, *J. Biomed. Mater. Res.* 57 (2001) 441.

Archieves of BioCeramics Research Volume 7
Proceeding of the Asian BioCeramics 2007, Osaka, Japan, 25-28 Sep. (2007)

Influence of Lubricant on Morphology of UHMWPE Debris in Hip Joint Simulator

Masami Hashimoto[a], Mineo Mizuno[b] and Satoshi Kitaoka[c]

Japan Fine Ceramics Center, Nagoya, Japan,
2-4-1 Mutsuno, Atsuta-ku, Nagoya, 456-8587, Japan
Tel. +81-52-871-3500, Fax +81-52-871-3599
[a]masami@jfcc.or.jp, [b]mizuno@jfcc.or.jp, [c]kitaoka@jfcc.or.jp

Keywords: Polyethylene debris; SEM analysis; Zirconia; Albumin; Globulin

Abstract. The protein concentration of various commercially available serum products varies in a wide range (40-80 mg/ml) and the protein concentration of lubricants has a marked effect on the friction and wear of tribological pairs used in prosthetic joints. In this study, the effect of the type of serum on the morphology of ultrahigh-molecular-weight polyethylene (UHMWPE) in a hip joint simulator has been investigated using computerized image analysis. The types of UHMWPE wear that occur in different types of bovine serum are similar each other. Quantitative analysis was then performed to develop a computational model that is useful in classifying particles. To develop a common vocabulary for describing particles, it is necessary to use this information.

Introduction

The ultimate goal in the design of a hip joint wear simulator and an associated test protocol is to produce the type and amount of wear that occurs clinically. Hip simulators that are commonly used vary markedly in load and motion characteristics, and use various lubricants, including distilled water, physiological saline, blood serum, synovial fluid, mineral oil and synthetic serum. Comparative studies have shown that the type and amount of wear that occurs in physiological lubricants (i.e., serum and synovial fluid) more closely resemble those occurring in vivo, probably due in part to boundary lubrication by proteins [1]. It has also been shown that the type and amount of wear vary with the type of protein present in the lubricant and the concentration of such protein.

At present, international standard recommends calf or bovine serum at pure concentration or diluted with distilled water as the best substitute for synovial fluid in *in vitro* tests, but there is no complete agreement concerning this choice. In fact, the protein concentration of various commercially available serum products varies in a wide range (40-80 mg/ml) and the protein concentration of lubricants has a marked effect on the friction and wear of tribological pairs used in prosthetic joints [2-3].

Owing to the importance of particle characteristics in the quantity and quality of biological responses, great emphasis has been given on developing techniques for extracting and studying the quantity, size and morphology of UHMWPE wear particles [4].

In this study, we analyzed UHMWPE particles using computerized image analysis to generate quantitative dimensions, and then categorize particles using subjective responses from individuals. Quantitative analysis was then performed to develop a computational model, that is, useful in classifying particles according in appropriate categories. This information may be useful for developing a common vocabulary for describing particles that incorporates both formal dimensions and subjective impression.

Materials and Methods

1) Materials and hip simulator

The wear behaviour of ZrO_2/UHMWPE coupling was investigated using a hip joint simulator. A ZrO_2 femoral head component with a diameter of 26 mm (Japan Medical Materials Corp., Osaka, Japan) was used as an acetabular component. The UHMWPE acetabular cup used was a commercial component of surgical implants (Japan Medical Materials Corp., Osaka, Japan). The inner and outer diameters of the UHMWPE cup were 26 mm and 50 mm, respectively. Two pieces for each condition were prepared.

A 12-station hip joint simulator (MTS Systems Corp., MN, USA) was used in the wear test. In the simulator, an acetabular cup was mounted above the femoral head in an upright position. Motion was imparted to the femoral head through an inclined rotating bearing block. This produced a cross-path pattern at all constant points on the articular interface. A physiological cyclic load was applied to the acetabular cup via a hydraulic acutuator mounted below the inclined block. Loads simulating a physiologic loading curve with double peaks of 1800 and 2800 N loads were applied. Loading and motion were synchronized at 1 Hz. Both the head and cup were completely immersed in 750 ml of fluid. The base lubricants used were calf -sera from two companies: Sigma-Aldrich Japan (Tokyo, Japan) (Serum A) and BioWest (Nuaill, France) (Serum B) (Table 1). A mixture of 25 vol% bovine serum, 20 mmol/L of ethylene diamine tetraacetic acid (EDTA), and 0.1 mass% sodium azide was used as lubricant, according to the ISO-14242-1 standard. Testing then continued until 5.0×10^6 cycles were completed.

2) Wear and surface characterization

All the lubricants were changed after every 0.5×10^6 cycles of testing. Between the lubricant changes, all the cups were cleaned, dried and weighed using an electronic balance (resolution: 0.01 mg) to determine weight loss. The cups were washed using a four-step procedure. First, the cups were cleaned in an ultrasonic bath for 10 min with a soap-water solution. Second, the cups were ultrasonically cleaned in deionized water for 10 min. Third, the cups were ultrasonically cleaned in ethanol for 10 min. Lastly, the cups were vacuum-dried for 30 min to remove excess water from the surface. Net weight losses for each cup were plotted against the number of test cycles

3) Debris extraction and SEM

A sample of the serum lubricant used in the simulator testing was obtained when the simulators were stopped for gravimetric analysis of wear performance. From the 750 ml lubricant bath, 10 ml was taken during the digestion and debris extraction. The homogeneity of the serum was confirmed by agitating the serum prior to sampling. In each case, synovial fluid was digested with the same amount of 10 M sodium hydroxide at 65 °C for 3 hours, applied to a sucrose (1.2 g/ml) and isopropyl alchol (0.919 g/ml) density gradient in a 30-ml tube, and ultracentrifuged at 25,200 rpm at 4 °C for 3 hours (Hitachi Koki Co, Ltd., Tokyo, Japan). The interface layer was collected and mixed with methyl -alcohol in another 30-ml tube, and ultracentrifuged again at 25,200 rpm for 3 hours. The bottom layer was applied to sucrose (1.05 g/ml) and isopropyl alchol density gradient (0.973 and 0.919 g/ml) and ultracentrifuged again at 25,200 rpm for 3 hours. UHMWPE debris were collected from the interface between the two layers and filtered through a 0.1-μm filter. The UHMWPE debris were examined using the field emission scanning electron microscopy (FE-SEM) system JSM-633OF (JEOL DATUM Co, Ltd., Nagoya, Japan) after coating them with a thin Au film.

4) Debris analysis

UHMWPE debris analysis was conducted on a computer using a custom application based on the public domain image-processing and analysis program, Image J. UHMWPE debris were outlined by binary image processing and analyzed to produce four shape and size parameters contained in R , E, AR and ECD for each particle. ECD is a measure of size defined as the diameter of a circle with an area equivalent to the area of the particle, and has units of length. Thus, the first area (A) of the particle is determined using image analysis and then ECD is calculated using

$$ECD = 2(A/\pi)^{1/2} \quad . \tag{1}$$

Aspect ratio (AR) is the rate of the major diameter to the minor diameter. Elongation (E) is the ratio of the particle's actual length to the particle's average width. Circularity (R) is a measure of how closely the particle resembles a circle, with a perfect circle having a value of 1.

Table 1 Compositions of serums used to lubricate wear tests

	Na	K	Ca	Cl	Protein (Total)	Albumin	Globulin			Alb/G
							α-G	β-G	γ-G	
Serum A (mg/ml)	3.38	NA	NA	NA	73	33.6	10.7	13.5	15.2	0.85
Serum B (mg/ml)	3.24	0.26	0.1	3.5	62.3	31.1	9.3	16.1	5.7	1

NA: Not available

Results and Discussion

Table 2 shows the change in the wear rate of the UHMWPE cups in the two serums. We defined the initial wear rate as that from the first cycle up to 1.0 x 10^{6th} cycle and steady wear rate as that from the 4.0 x 10^{6th} cycle to the 5.0 x 10^{6th} cycle. The initial wear rate of the UHMWPE cup in serum A was -27.9 mg/10^6 cycles; the steady wear rate of the same UHMWPE cup increased to -41.41 mg/10^6 cycles. In contrast, those of the UHMWPE cup in serum B decreased to -16.93 and -12.82 mg/10^6 cycles, respectively.

Table 2 Wear rates of UHMWPE cup in hip joint simulator tests

Serum	Initial wear rate (mg/10^6 cycles)	Steady wear rate. (mg/10^6 cycles)
Serum A	-27.9	-41.41
Serum B	-16.93	-12.82

Figure 1 shows SEM photographs of UHMWPE debris isolated from the lubricant after a 5 x 10^6 -cycle simulator test. It was revealed that the number of wear debris isolated from Serum A was larger than that of wear debris isolated from Serum B. This result is consistent with the wear rate result.

The results of quantitative analysis of UHMWPE debris generated in serums A and B are presented in Tables 2 and 3, respectively. Mean ECD, AR, E and R values significantly differed among the particle types. However, these values of UHMWPE debris in serum A (Table 3) were equal to those of UHMWPE debris in serum B (Table 4).

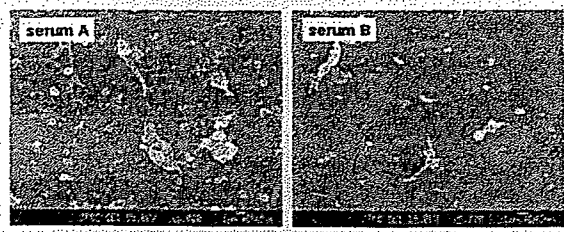

Figure 1 SEM photographs of UHMWPE debris

Table 3 Size and shape descriptors of UHMWPE wear debris in Serum A

	N	ECD (μm)	AR	E	R
Fiber	56,550	0.54±0.49	3.66±1.53	1.95±2.05	0.34±0.11
Flake	38,100	0.29±0.19	2.74±0.65	0.87±0.51	0.56±0.05
Granule	118,725	0.21±0.11	2.25±0.45	0.59±0.27	0.84±0.10
Total	213,375	0.31±0.31	2.71±1.08	1.00±1.24	0.66±0.24

Table 4 Size and shape descriptors of UHMWPE wear debris in Serum B

	N	ECD (μm)	AR	E	R
Fiber	12,675	0.60±0.73	4.17±1.99	2.14±2.73	0.34±0.11
Flake	11,400	0.31±0.22	2.88±0.71	0.85±0.55	0.59±0.05
Granule	34,350	0.26±0.14	2.14±0.55	0.63±0.30	0.85±0.09
Total	58,425	0.34±0.39	2.73±1.34	1.00±1.44	0.69±0.23

Summary

This hip joint simulator study demonstrated that the protein concentration of a serum has a marked effect on the wear performance of UHMWPE cups. As albumin/globulin protein ratio increased, UHMWPE wear rate decreased. A comparison of the quantitative measurements of the isolated UHMWPE debris from two serums showed that the amount of wear considerably differed between the serums. However, the types of UHMWPE debris that formed in the two serums were almost the same.

References

[1] Y.S. Liao, H. McKellop, Z. Lu, P. Campbell, P. Benya: Biomaterials Vol.24 (2003), p. 3047.

[2] I.C. Clarke, F.W. Chan, A. Essner, V. Good, C. Kaddick: Wear Vol.250 (2001), p. 188.

[3] M.P. Heuberger, M.R. Widmer, E. Zobeley, R. Glockshuber, N.D. Spencerl: Biomaterials Vol.26 (2005), p. 1165.

[4] B.T. McMullin, M.Y. Leung, A.S. Shanbhag, D. McNulty, J.D. Mabrey, C.M. Agrawal: Biomaterials Vol.27 (2006), p. 752.

Available online at www.sciencedirect.com
ScienceDirect
Materials Science and Engineering C 27 (2007) 206–212
MATERIALS SCIENCE & ENGINEERING C
www.elsevier.com/locate/msec

Electrodeposition of amine-terminated poly(ethylene glycol) to titanium surface

Yuta Tanaka [a,b], Hisashi Doi [a], Yasuhiko Iwasaki [a], Sachiko Hiromoto [c], Takayuki Yoneyama [a], Katsuhiko Asami [d], Hachiro Imai [b], Takao Hanawa [a,*]

[a] *Institute of Biomaterials and Bioengineering, Tokyo Medical and Dental University, Tokyo 101-0062, Japan*
[b] *Department of Materials Science and Technology, Shibaura Institute of Technology, Tokyo 108-8548, Japan*
[c] *Biomaterials Center, National Institute for Materials Science, Tsukuba 305-0044, Japan*
[d] *Institute of Materials Research, Tohoku University, Sendai 980-8577, Japan*

Received 8 July 2005; accepted 3 March 2006
Available online 23 June 2006

Abstract

The immobilization of poly(ethylene glycol), PEG, to a solid surface is useful to functionalize the surface, e.g., to prevent the adsorption of proteins. No successful one-stage technique for the immobilization of PEG to base metals has ever been developed. In this study, PEG in which both terminals or one terminal had been modified with amine bases was immobilized onto a titanium surface using electrodeposition. PEG was dissolved in a NaCl solution, and electrodeposition was carried out at 310 K with −5 V for 300 min. The thickness of the deposited PEG layer was evaluated using ellipsometry, and the bonding manner of PEG to the titanium surface was characterized using X-ray photoelectron spectroscopy after electrodeposition. The results indicated that a certain amount of PEG was adsorbed on titanium through both electrodeposition and immersion when PEG was terminated by amine. However, terminated amines existed at the surface of titanium and were combined with titanium oxide as N–HO by electrodeposition, while amines randomly existed in the molecule and showed an ionic bond with titanium oxide by immersion. The electrodeposition of PEG was effective for the inhibition of albumin adsorption. This process is useful for materials that have electroconductivity and a complex morphology.

Keywords: Titanium; PEG; Immobilization; Electrodeposition; Surface analysis

1. Introduction

The demand for metals in medical and dental devices is large. These materials are used because of their high durability, strength, and formability. Conventionally, metals are essential for orthopedic implants, bone fixators, artificial joints, and external fixators, since they can substitute for the mechanical function of hard tissues in orthopedics. In other words, metals in medical devices cannot be replaced with ceramics or polymers at present, mainly because the metallic materials have greater strength and toughness. On the other hand, metallic materials are generally not expected to be the biomaterials of the future at the research level because they do not have bioactive and biofunctional properties.

However, metals with biofunctions have been required in the recent past. For example, stents are placed at stenotic blood vessels for dilatation, and blood compatibility or prevention of adhesion of platelets is necessary. In guide wires and guiding catheters, lubrication in the blood vessels is important for proper sliding and insertion. In addition, if metals are used as sensing devices, the control of cell adhesion is necessary. For these purposes, the fundamental property is the inhibition of protein adsorption. Poly (ethylene glycol), PEG, is a biofuctional molecule on which the adsorption of proteins is inhibited. Therefore, the immobilization of PEG to a metal surface is an important step towards the biofunctionalization of the metal surface.

The immobilization of biofunctional polymers on a noble metals such as gold is usually conducted by using the bonding –SH or –SS-group; however, this technique can only be used

* Corresponding author. Tel.: +81 3 5280 8006; fax: +81 3 5280 8011.
E-mail address: hanawa.met@tmd.ac.jp (T. Hanawa).

0928-4931/$ - see front matter © 2006 Elsevier B.V. All rights reserved.
doi:10.1016/j.msec.2006.03.007

for noble metals. The adhesion of platelets and adsorption of proteins, peptides, antibodies, and DNA is controlled by modifications of the above technique. On the other hand, a class of copolymers based on poly (L-lysine)-g-poly (ethylene glycol), PLL-g-PEG, has been found to spontaneously adsorb from aqueous solutions onto TiO_2, $Si_{0.4}Ti_{0.6}O_2$, and Nb_2O_5 to develop blood-contacting materials and biosensors [1,2]. In another case, TiO_2 and Au surfaces are functionalized by the attachment of poly(ethylene glycol)-poly(DL-lactic acid), PEG–PLA, copolymeric micelles. The micelle layer can enhance the protein resistance of the surfaces up to 70% [3]. Peptides with terminal cysteine residues were immobilized on maleimide-activated oxides [4–6]. A surface of stainless steel was firstly modified by a silane-coupling agent, SCA, (3-mercaptopropyl)trimethoxysilane. The silanized stainless steel, SCA-SS, surface was subsequently activated by argon plasma and then subjected to UV-induced graft polymerization of poly (ethylene glycol)methacrylate, PEGMA. The PEGMA graft-polymerized stainless steel coupon, PEGMA-g-SCA-SS, with a high graft concentration and, thus, a high PEG content was found to be very effective to prevent the absorption of bovine serum albumin and γ-globulin [7]. These processes require several steps but are effective for immobilization; however, no promising technique for the immobilization of PEG to a metal surface has been so far developed.

In this study, PEG in which both terminals or one terminal had been modified with amine bases was immobilized onto a titanium surface by electrodeposition in an attempt to develop a new technique that could be used for all metals and complexly designed surfaces. Furthermore, the mode of immobilization and chemical bonding state was characterized using X-ray photoelectron spectroscopy, XPS. The adsorption of plasma protein on the PEG-immobilized surface was evaluated.

2. Experimental

2.1. Electrodeposition

Both terminals of PEG were terminated with $-NH_2$ (B-PEG; PEG1000 Diamine, NOF Corporation, Japan), and only one terminal was terminated with $-NH_2$ (O-PEG; SUNBRIGHT MEPA-10H, NOF Corporation, Japan). The chemical structures of the PEGs are shown in Fig. 1. The molecular weights of both PEGs

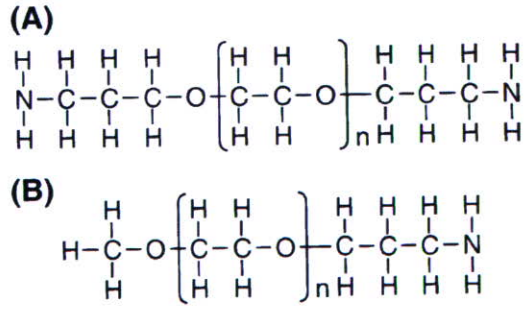

Fig. 1. Chemical structures of PEGs in which both terminals (A) and one terminal (B) were terminated with amine.

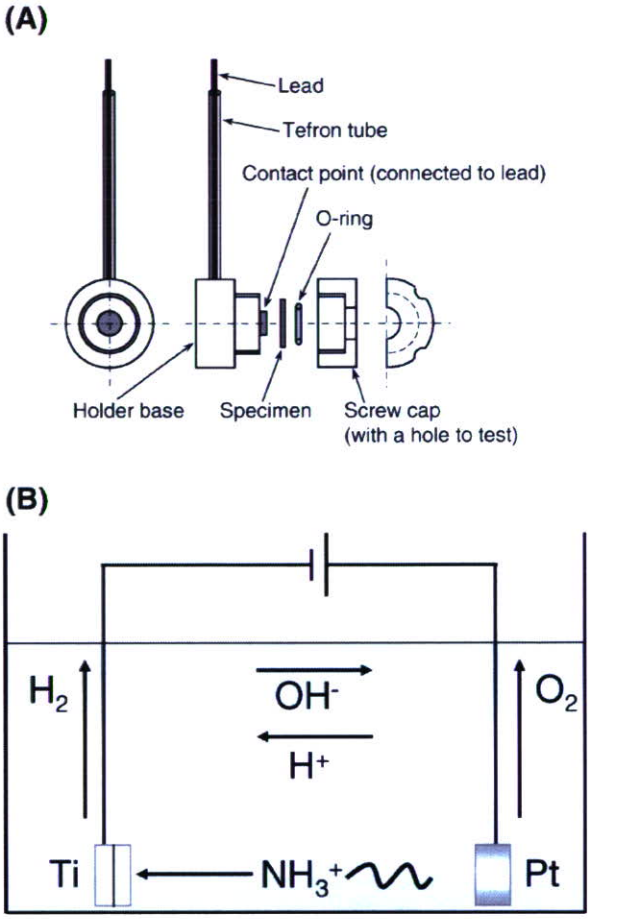

Fig. 2. Design of a polytetrafluoroethylene holder of titanium for electrodeposition (A) and schematic illustration of electrodeposition.

were about 1000. These terminated PEGs were dissolved in a 0.3-mol L^{-1} NaCl solution with a concentration of 2 mass%. In the solution, the $-NH_2$ terminal was dissociated and charged as $-NH_3^+$. The pH of the solution with B-PEG was 11.2, and that of the solution with O-PEG was 11.0. The resultant solution was used as an electrolyte for electrodeposition at 310 K.

A commercially pure titanium disk (8 mmϕ × 2 mm in thickness) with grade 2 was metallographically polished and ultrasonically rinsed in acetone and deionized water (Milipore). The titanium disk was fixed in a polytetrafluoroethylene holder that was insulated from the electrolyte except for an opening made for electrodeposition (6.0 mmϕ), as shown in Fig. 2(A). Therefore, the area exposed for electrodeposition was 28.3 mm^2. The open circuit potential of titanium, E_{open}, vs. a saturated calomel electrode, SCE, before electrodeposition was measured as *ca.* −0.5 V. Thereafter, the cathodic potential was charged from E_{open} to −5 V vs. SCE with a sweep rate of 0.1 V s^{-1} and maintained at this potential for 300 s. During charging, the terminated PEGs were electrically migrated to the titanium cathode and deposited on it as shown in Fig. 2(B). This cathodic current was measured during electrodeposition and compared with the results from the NaCl solution without PEG. For comparison, titanium was immersed in the electrolyte containing B-PEG for 2 h and 24 h without any electric charge at 310 K. After electrodeposition,

specimens were rinsed in deionized water and dried with a stream of nitrogen gas (99.9%).

2.2. Ellipsometry

The thickness of the PEG layer deposited on titanium was determined with an ellipsometer (DVA-36Ls, Mizojiri Optical Co., Ltd.) in air. The use of an ellipsometer resulted in the underestimation of the thickness compared to that in solution. The light source was a He–Ne laser with a wavelength of 632.8 nm, and the incident angle to the titanium surface was 70°. The thickness was calculated by optical constants: the refractive index and absorption coefficient of titanium oxide with the titanium substrate were 2.209 and 3.079 [8,9], and those of the titanium substrate were 2.22 and 2.99 [10], respectively.

2.3. XPS

The deposition mode of PEG to the titanium surface and the chemical bonding state were characterized using XPS (SSI-SSX100). The take-off angle for photoelectron detection was 35° from the surface of the specimen. All binding energies given in this paper are relative to the Fermi level, and all spectra were excited with the monochromatized Al Kα line (1486.61 eV). The spectrometer was calibrated against Au $4f_{7/2}$ (binding energy, 84.07 eV) and Au $4f_{5/2}$ (87.74 eV) of pure gold and Cu $2p_{3/2}$ (932.53 eV), Cu $2p_{1/2}$ (952.35 eV), and Cu Auger $L_3M_{4,5}M_{4,5}$ line (kinetic energy, 918.65 eV) of pure copper. The energy values were based on published data [11]. In order to estimate the photoelectron peak intensities, the background was subtracted from the measured spectrum according to Shirley's method [12]. The composition and thickness of the surface oxide and the composition of the substrate were simultaneously calculated according to a method devised by one of the authors of this study [13,14]. Empirical data [15] and theoretically calculated data [16] of relative photoionization cross-sections were used for the quantification. The relative photoionization cross-sections used in this study are summarized in Table 1, where $\sigma ij/\sigma_{O\ 1s}$ represents the relative photoionization cross-section of a level j electron of an element i to that of O 1s electrons.

2.4. Adsorption of albumin

The inhibition of plasma protein adsorption to a titanium surface with PEG deposition was evaluated. Albumin (fluorescein isothiocyanate conjugated bovine, A9771, Sigma) was dissolved into phosphate-buffered saline without calcium chloride and magnesium chloride (PBS: Dulbecco's PBS, D1408, Sigma) with a concentration of 4.5 g L^{-1}. Specimens were immersed in albumin-containing PBS for 30 min, rinsed with PBS and deionized water, and then dried with a stream of nitrogen gas (99.9%). The surface of specimens was observed with a fluorescence microscope (E-600, Nikon).

Table 1
Photoionization cross-sections of level j of element i relative to that of O 1s, $\sigma_{ij}/\sigma_{O\ 1s}$

Photoionization cross-section			
Level	Ti $2p_{3/2}$	C 1s	N 1s
σ_{ij}	1.28	0.34	0.62
Reference	14	15	15

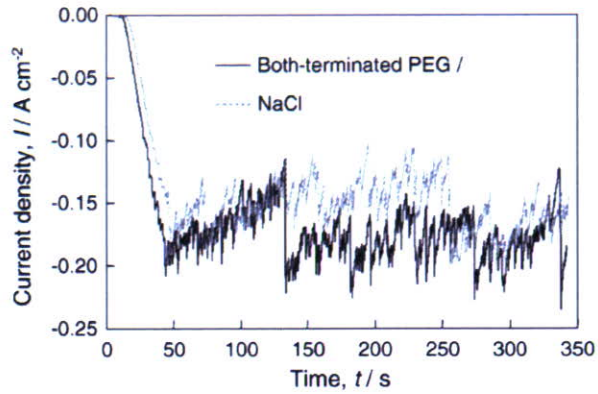

Fig. 3. Cathodic current during electrodeposition in NaCl solutions with and without PEG in which both terminals were terminated.

3. Results and discussion

3.1. Cathodic current

The cathodic current increased with the decrease of the potential in the cathodic direction and became almost constant after reaching the target potential, −5 V, with irregularities between −0.15 and −0.20 A cm^{-2}, as shown in Fig. 3. These current values contain a hydrogen evolution current because the charged potential was much lower than that of the hydrogen evolution potential according to the Pourvaix diagram [17]. The passive oxide film on titanium is not electrically reduced because hydrogen evolution is preferential even though the charged potential is within the range of immunity. In addition, the cathodic current in the NaCl solution without PEG was almost the same as that in

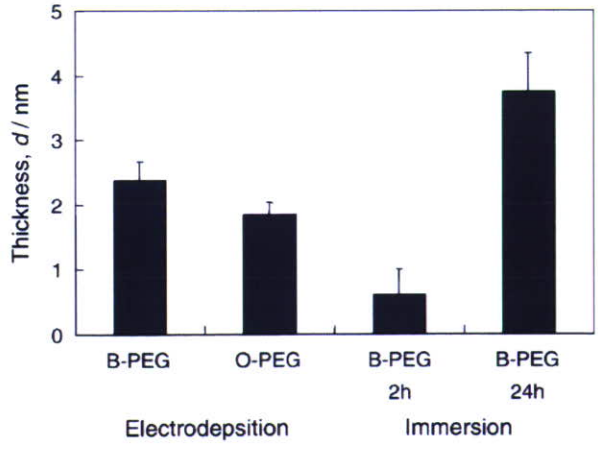

Fig. 4. Thickness of the PEG layer deposited on titanium by electrodeposition and immersion. B-PEG: both-terminal-modified PEG. O-PEG: one-terminal-modified PEG.

Table 2
Relative concentrations of elements determined by XPS

Deposition process	PEG termination Deposition time	Concentration (mass%) C	O	N	Ti
Electrodeposition	Both-terminal 300 s	41.8 (0.4)*	44.4 (0.3)	1.3 (0.3)	12.5 (0.2)
	One-terminal 300 s	45.9 (1.0)	41.8 (0.8)	1.3 (0.1)	10.9 (0.3)
Immersion	Both-terminal 2 h	49.3 (1.5)	41.8 (0.5)	1.5 (0.0)	13.5 (1.0)
	Both-terminal 24 h	45.8 (1.7)	41.2 (1.3)	2.2 (0.0)	10.9 (0.5)

The bars in the table represent significant differences between the corresponding values ($p<0.05$).

the solution with PEG. Therefore, an electrodeposition phenomenon did not clearly appear on the current.

3.2. Thickness of adsorbed PEG by ellipsometry

Fig. 4 shows the thicknesses of the PEG deposition layers determined by ellipsometry. These thicknesses are measured in air; therefore, the real thickness in solutions is larger than these values. The thickness of the deposition layer, in other words, the amount of deposited PEG, is the largest in this order: 24 h-immersion B-PEG, electrodeposition of B-PEG for 300 s, electrodeposition of O-PEG for 300 s, and 2 h-immersion B-PEG. This indicated that electrodeposition was more effective than immersion for the deposition of PEG on the titanium surface. However, the PEG layer increased after a 24 h-immersion, indicating that the charged terminals of PEG attracted the electrostatically titanium surface that is covered by titanium oxide with a large number of hydroxyl groups [18,19]. In electrodeposition, the thickness of the B-PEG deposition layer was larger than that of the O-PEG deposition layer. This does not necessarily indicate that more B-PEG than O-PEG was deposited because ellipsometry was conducted in air and the PEG molecules collapsed on titanium. The B-PEG has more density per molecule after deposition on titanium surface than the O-PEG because both terminals are attracted to the titanium surface in the B-PEG. Therefore, the apparent thickness of the B-PEG in air was larger than that of the O-PEG.

3.3. Concentrations of elements by XPS

Carbon, nitrogen, oxygen, and titanium were detected using XPS. The relative concentrations of carbon, nitrogen, oxygen, and titanium in specimens were calculated assuming that the gross amount of these elements, as detected using XPS, was 100 mol%. Table 2 presents the concentrations of elements. Sodium and chlorine were not detected.

The carbon concentration was governed by the amount of PEG existing on titanium because carbon atoms exist in the whole molecule. Therefore, the difference in the carbon concentration represented that in the deposition amount of PEG. When a large amount of PEG was deposited on titanium, the apparent concentration of titanium decreased in the determination with XPS. The results of the titanium concentration are in good agreement

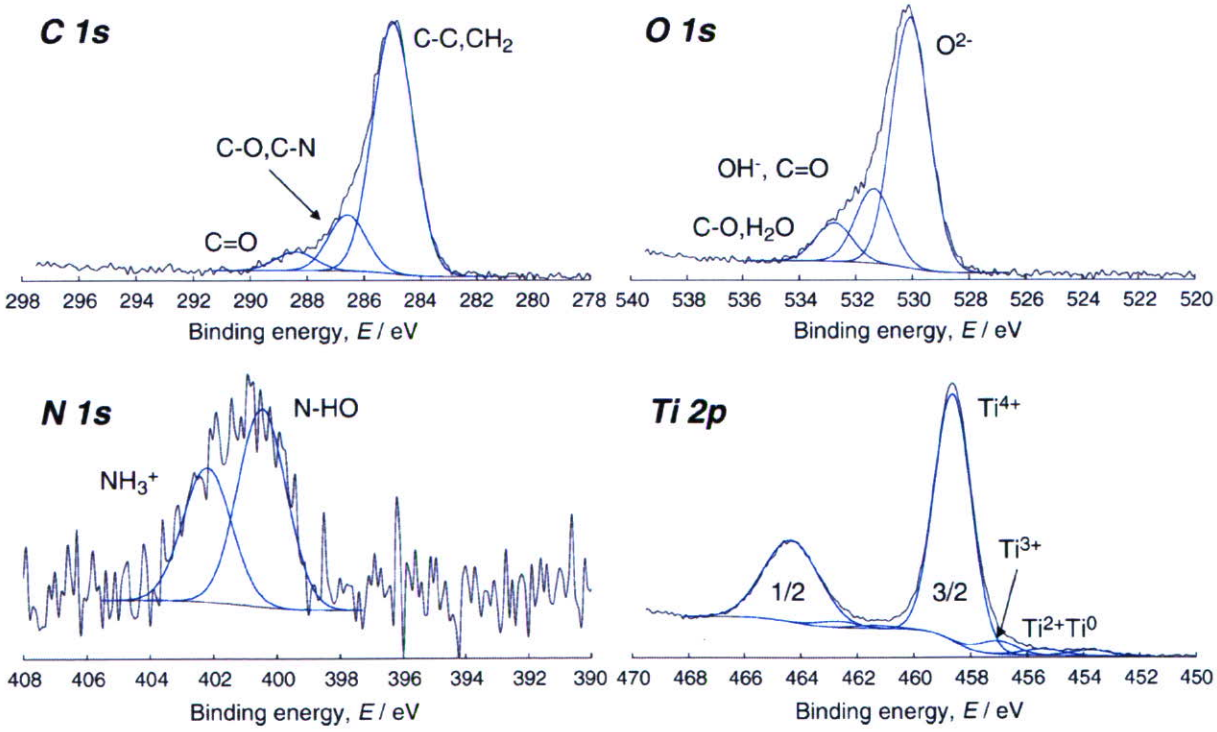

Fig. 5. C 1 s, O 1 s, N 1 s, and Ti 2p electron energy region spectra by XPS and deconvolution of the peaks to component peaks.

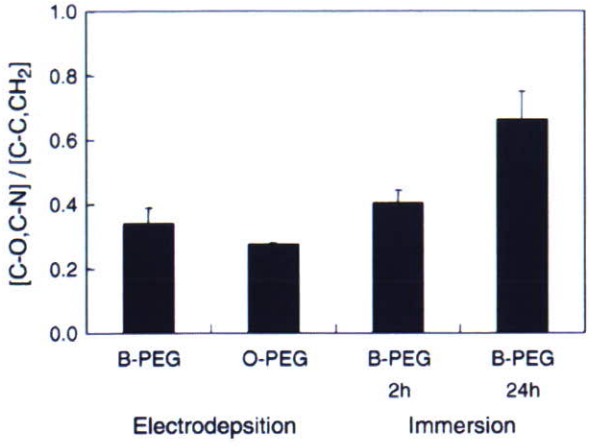

Fig. 6. Ratio, [C–O,C–N]/[C–C,CH], obtained from the deconvoluted C 1s electron energy region peak. B-PEG: both-terminal-modified PEG. O-PEG: one-terminal-modified PEG.

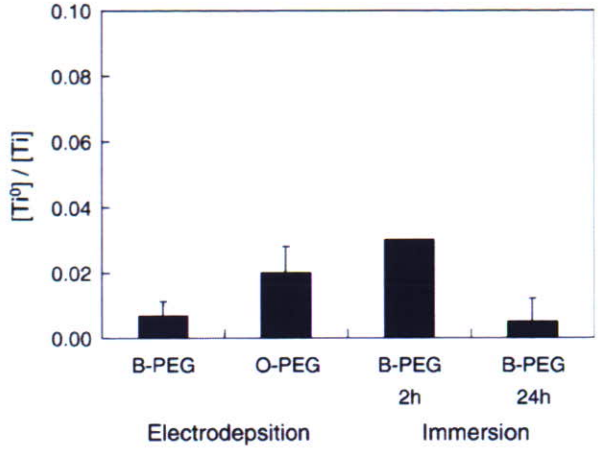

Fig. 8. Ratio, [Ti^0]/[Ti], obtained from the deconvoluted Ti 2p electron energy region peak. B-PEG: both-terminal-modified PEG. O-PEG: one-terminal-modified PEG.

with those of the carbon concentration from the viewpoint of the relative magnitude of both element concentrations. The carbon concentration in the electrodeposition of the O-PEG was significantly larger than that in the B-PEG, indicating that more O-PEG than B-PEG was deposited on titanium by electrodeposition. Probably, the B-PEG occupies more deposition sites, *e.g.*, hydroxyl groups on titanium oxide, than the O-PEG and less B-PEG could be deposited on titanium because B-PEG contains twice as many electric charges as O-PEG. More B-PEG adsorbed on titanium in a 24 h-immersion than in electrodeposition. In other words, PEG can be deposited on titanium only by long-time immersion whenever PEG is terminated by amine, independently of the mode of adsorption or chemical bond.

On the other hand, the nitrogen concentration in the 24 h-immersion specimen was significantly larger than those of other specimens. Nitrogen is originated from the terminal amines in PEG. The photoelectron signals detected by XPS from a deep site are weak because they decay while passing through molecules and solids. Therefore, nitrogen atoms in electrodeposited specimens and 2 h-immersed specimens were located at deeper sites than 24 h-immersed specimens.

3.4. Chemical states of elements and bonding manner

Typical XPS spectra of C 1s, O 1s, N 1s, and Ti 2p electron energy regions and the deconvolutions of these peaks are shown in Fig. 5 [20–26].

The ratio, [C–O, C–N]/[C–C, CH_2], in the C 1s peak in each specimen is shown in Fig. 6. C–C bonds existed in the entire molecule of PEG; therefore, this ratio is governed by the C–N bond. The photoelectron signals in XPS abruptly decayed depending on the depth direction. Therefore, the C–N bond was located inside of the deposited PEG layer by electrodeposition more often than by immersion because C–N bonds exist only at the terminal and C–O bonds exist in the whole molecule. In other words, nitrogen atoms exist at the interface between PEG and titanium.

The change in the ratios, [NH_3^+]/[N–HO], in the N 1s peak is shown in Fig. 7. This ratio is much smaller in electrodeposited

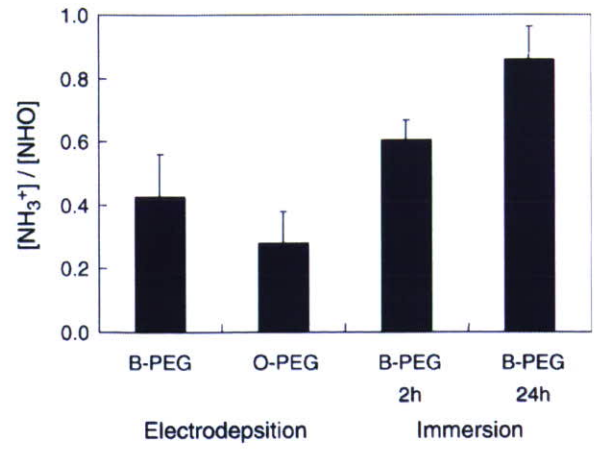

Fig. 7. Ratio, [NH_3^+]/[N–HO], obtained from the deconvoluted N 1s electron energy region peak. B-PEG: both-terminal-modified PEG. O-PEG: one-terminal-modified PEG.

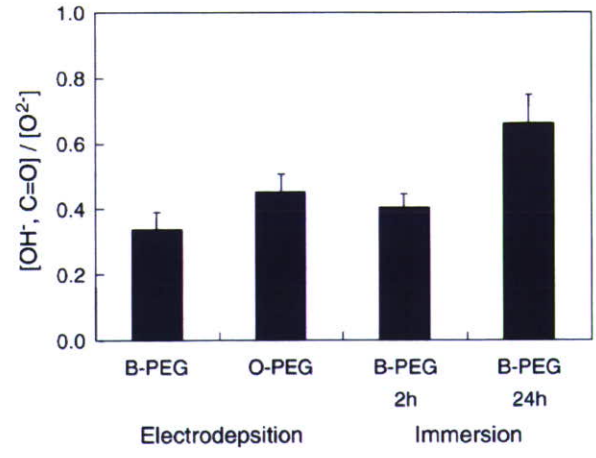

Fig. 9. Ratio, [OH^-, C=O]/[O^{2-}], obtained from the deconvoluted O 1 s electron energy region peak. B-PEG: both-terminal-modified PEG. O-PEG: one-terminal-modified PEG.

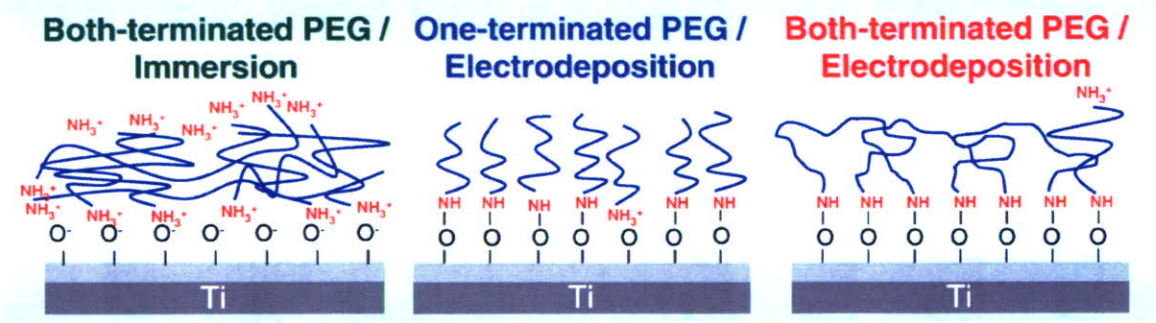

Fig. 10. Schematic model of the deposition mode and chemical bonding state of PEG by immersion and electrodeposition.

specimens than in immersed specimens. Nitrogen atoms in electrodeposited specimens existed as a N–HO bond rather than as NH_3^+. This indicated that strong bonding between amine and titanium oxide was formed by electrodeposition, while ionic bonding was formed by immersion.In the Ti 2p region spectrum, the Ti^0 peak originates from the titanium metal substrate, and Ti^{2+}, Ti^{3+}, and Ti^{4+} peaks originate from titanium surface oxide. The integrated intensity of Ti^{4+} was the largest: titanium surface oxide is mainly TiO_2. Although the proportion of Ti^{4+} among the Ti $2p_{3/2}$ peaks was almost constant, that of Ti^0 varied according to the specimen preparation conditions, as shown in Fig. 8. When the adsorbed layer of PEG was thick, the intensity of Ti^0 decreased because the signal from the titanium substrate was small. In this sense, the magnitude of the proportion shown in Fig. 8 is completely in accordance with the results from ellipsometry in Fig. 4.

From the decomposition of the O 1s peak, a large amount OH^- existed in the 24 h-immersion specimen (Fig. 9). Probably, adsorbed PEG contained a large amount of OH^-, whereas titanium oxide surface contains OH^- [18,19]. The amount was larger in the 24 h-immersed specimen than in the 2 h-immersed specimen, resulting in the difference in the amount of deposited PEG.

A certain amount of PEG is deposited on titanium through both electrodeposition and immersion when PEG is terminated by amine and charged in an aqueous solution. However, terminated amines exist at the surface of titanium and are combined with titanium oxide as N–HO bond by electrodeposition, while amines randomly exist in the PEG layer and show an ionic bond with titanium oxide by immersion. In the B-PEG, the PEG deposited as a U-shape because both terminals combined with the titanium surface; in the O-PEG, PEG was deposited as a brush because only one terminal was combined with the surface. These results are illustrated in Fig. 10.

3.5. Albumin adsorption

Fig. 11 shows fluorescent images of albumin adsorbed on titanium before and after immobilization of PEG. The adsorption of albumin was inhibited with the deposition of PEG. Therefore, the electrodeposition of PEG was effective for the inhibition of the adsorption of albumin.

4. Conclusions

A certain amount of PEG was adsorbed on titanium through both electrodeposition and immersion when PEG is terminated by amine. However, terminated amines exist at the surface of titanium and are combined with titanium oxide as N–HO by electrodeposition, while amines randomly exist in the molecule and show an ionic bond with titanium oxide by immersion. The both-terminal-terminated PEG is deposited as a U-shape, and the one-terminal-terminated PEG is deposited as a brush. The

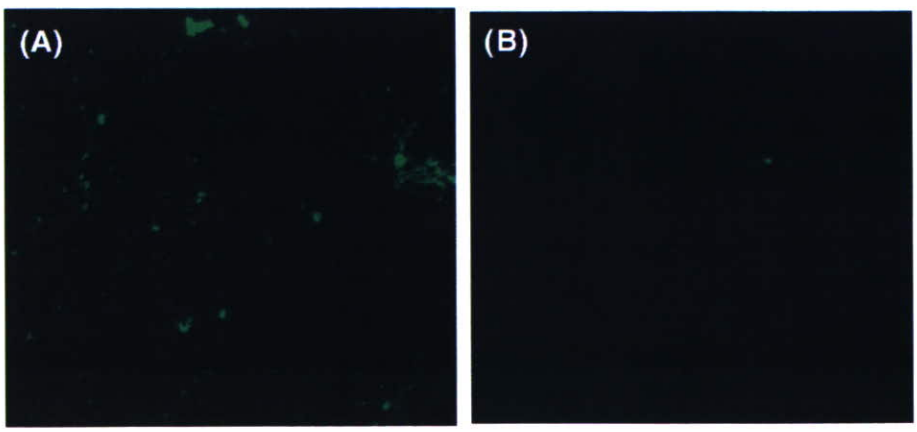

Fig. 11. Fluorescent images of albumin adsorbed on titanium before (A) and after (B) deposition of PEG.

electrodeposition of PEG was effective for the inhibition of albumin adsorption. This immobilization process is useful for all electroconductive and morphological materials.

References

[1] G.L. Kenausis, J. Vörös, D.L. Elbert, N. Huang, R. Hofer, L. Ruiz-Taylor, M. Textor, J.A. Hubbell, N.D. Spencer, J. Phys. Chem., B 104 (2000) 3298.
[2] N.P. Huang, R. Michel, J. Vörös, M. Textor, R. Hofer, A. Rossi, D.L. Elbert, J.A. Hubbell, N.D. Spencer, Langmuir 17 (2001) 489.
[3] N.P Huang, G. Csucs, K. Emoto, Y. Nagasaki, K. Kataoka, M. Textor, N.D. Spencer, Langmuir 18 (2002) 252.
[4] S.J. Xiao, M. Textor, N.D. Spencer, H. Sigrist, Langmuir 114 (1998) 5507.
[5] S.J. Xiao, M. Textor, N.D. Spencer, M. Wieland, B. Keller, H. Sigrist, J. Mater. Sci., Mater. Med. 8 (1997) 867.
[6] A. Rezania, R. Johnson, A.R. Lefkow, K.E. Healy, Langmuir 15 (1999) 6931.
[7] F. Zhang, E.T. Kang, K.G. Neoh, P. Wang, K.L. Tan, Biomaterials 22 (2001) 1541.
[8] CRC Handbook of Chemistry and Physics, 67th ed., CRC Press, Boca Raton, Florida, 1986, p. E-389.
[9] E.D. Palik (Ed.), Handbook of Optical Constants of Solids, Academic Press, 1985, p. 233.
[10] E.D. Palik (Ed.), Handbook of Optical Constants of Solids, Academic Press, 1985, p. 795.
[11] K. Asami, J. Electron Spectrosc. 9 (1976) 469.
[12] D.A. Shirley, Phys. Rev., B 5 (1972) 4709.
[13] K. Asami, K. Hashimoto, S. Shimodaira, Corros. Sci. 17 (1977) 713.
[14] K. Asami, K. Hashimoto, Corros. Sci. 24 (1984) 83.
[15] K. Asami, S.-C. Chen, H. Habazaki, A. Kawashima, K. Hashimoto, Corros. Sci. 31 (1990) 727.
[16] J.H. Scofield, J. Electron Spectrosc. 8 (1976) 129.
[17] M. Pourbaix, Atlas of Electrochemical Equilibria in Aqueous Solution, National Association of Chemical Engineers, Houston, TX, 1974.
[18] T. Hanawa, K. Asami, K. Asaoka, J. Biomed. Mater. Res. 40 (1998) 530.
[19] S. Hiromoto, T. Hanawa, K. Asami, Biomaterials 25 (2004) 979.
[20] B. Lindberg, R. Maripuu, K. Siegbahn, R. Larsson, C.-G. Gölander, J.C. Eriksson, J. Colloid Interface Sci. 95 (1983) 308.
[21] T. Solomun, A. Schimanski, H. Sturm, E. Illenberger, Chem. Phys. Lett. 387 (2004) 312.
[22] I. Losito, C. Malitesta, I.D. Bari, C.-D. Calvano, Thin Solid Film. 473 (2005) 104.
[23] K.M. Hansson, S. Tosatti, J. Isaksson, J. Wetterö, M. Textor, T.L. Lindahl, P. Tengvall, Biomaterials 26 (2005) 861.
[24] K. Asami, K. Hashimoto, Corros. Sci. 17 (1977) 559.
[25] M. Yabe, Adv. X-ray Chem. Anal. Jpn. 17 (1986) 71.
[26] K. Asami, S.-C. Chen, H. Habazaki, K. Hashimoto, Corros. Sci. 35 (1993) 43.

Available online at www.sciencedirect.com
ScienceDirect
Biomaterials 28 (2007) 984–993
Biomaterials
www.elsevier.com/locate/biomaterials

Enzyme-degradable phosphorylcholine porous hydrogels cross-linked with polyphosphoesters for cell matrices

Chookaet Wachiralarpphaithoon[a], Yasuhiko Iwasaki[a,*], Kazunari Akiyoshi[a,b]

[a]*Institute of Biomaterials and Bioengineering, Tokyo Medical and Dental University, 2-3-10 Kanda-surugadai, Chiyoda-ku, Tokyo 101-0062, Japan*
[b]*Center of Excellence Program for Frontier Research on Molecular Destruction and Reconstruction of Tooth and Bone, Tokyo Medical and Dental University, 2-3-10 Kanda-surugadai, Chiyoda-ku, Tokyo 101-0062, Japan*

Received 14 August 2006; accepted 24 October 2006
Available online 14 November 2006

Abstract

Biodegradable highly porous hydrogels composed of poly [2-methacryloyloxyethyl phosphorylcholine (MPC)] cross-linked with polyphosphoesters have been prepared as novel cellular matrices. Well-controlled porous hydrogels were fabricated by using potassium hydrogen carbonate as a porogen salt for forming gas. This process enabled the homogeneous expansion of pores within the polymer hydrogel matrices, leading to well-interconnected high porosity. The mechanical properties of the hydrogels were influenced by the cross-linking density and porous structure. Hydrolysis and enzymatic digestion of the hydrogels were determined under basic conditions. The cross-linking density and porosity influenced the rate of degradation of the hydrogels. Acceleration of the degradation with alkaline phosphatase was also observed. Cultivation of mouse osteoblastic cell (MC3T3-E1) was performed in the highly porous hydrogels and cell viability was well maintained. The rate of cell proliferation also was relatively increased with an increase in the amount of polyphosphoesters in the hydrogel. Basic fibroblast growth factor (bFGF) was physically absorbed by the hydrogels and effectively induced cell proliferation. In conclusion, the porous hydrogels prepared in this study contributed a suitable environment for three-dimensional cell cultivation and may be useful for cell and tissue matrices.

Keywords: Porous hydrogels; Biodegradable polymers; Polyphosphoesters; Growth factors; Tissue engineering

1. Introduction

Biomaterials have an enormous impact on human health care. They are widely used in biomedical applications, including drug delivery devices and tissue-engineering matrices [1]. Specifically, hydrogels are included in the more recent trend of biomaterials because they can absorb significant amounts of water and are as flexible as soft tissue, which minimize their potential for irritation of surrounding tissue. While various types of hydrogels have been proposed as synthetic cellular matrices [2–5], designs offering both biocompatibility and biodegradability are still limited.

Polyphosphoesters are a recent candidate as biodegradable polymers, which have been synthesized with various processes such as ring-opening polymerization [6,7], polycondensation [8], transesterification [9,10], and enzymatic polymerization [11]. Polyphosphates have been of interest for tissue engineering and gene delivery applications [12–14]. Quite recently, Li and coworkers have synthesized photocrosslinkable a phosphoester hydrogel that induces mineralization of bone marrow-derived mesenchymal stem cells [15]. Because the ultimate hydrolysis products are phosphate ions, alcohol, and a diol, the polymer has the potential of being nontoxic [16].

For synthetic extracellular matrices, cellular adhesion capacity and incorporation of growth factors must induce cell growth in the matrices in the same manner as natural extracellular matrices [17]. Recently, numerous types of growth factors have been identified and used in controlling cell growth. However, it should be noted that growth factors are generally very sensitive to external environmental factors and unfavorable adsorption on biomaterials

*Corresponding author. Tel.: +81 3 5280 8026; fax: +81 3 5280 8027.
E-mail address: yasu.org@tmd.ac.jp (Y. Iwasaki).

0142-9612/$ - see front matter © 2006 Elsevier Ltd. All rights reserved.
doi:10.1016/j.biomaterials.2006.10.024